A General Strategy for Biocompatible, High-Effective Upconversion Nanocapsules Based on Triplet−Triplet Annihilation

Qian Liu,[†,#] Baoru Yin,[‡,#] Tianshe Yang,[†] Yongchao Yang,[§] Zhen Shen,[§] Ping Yao,[‡] and Fuyou Li*[,†]

[†]Department of Chemistry & The State Key Laboratory of Molecular Engineering of Polymers & Institute of Biomedicine Science, Fudan University, Shanghai, 200433, P. R. China

[‡]The State Key Laboratory of Molecular Engineering of Polymers & Department of Macromolecular Science, Fudan University, Shanghai, 200433, P. R. China

[§]School of Chemistry and Chemical Engineering, Nanjing University, Nanjing 210093, P. R. China

Ⓢ *Supporting Information*

ABSTRACT: A general strategy for constructing high-effective upconversion nanocapsules based on triplet−triplet annihilation (TTA) was developed by loading both sensitizer and annihilator into BSA−dextran stabilized oil droplets. This strategy can maintain high translational mobility of the chromophores, avoid luminescence quenching of chromophore by aggregation, and decrease the O_2-induced quenching of TTA-based upconversion emission. Pt(II)-tetraphenyl-tetrabenzopor-phyrin (PtTPBP) and BODIPY dyes (BDP-G and BDP-Y with the maximal fluorescence emission at 528 and 546 nm, respectively) were chosen as sensitizer/annihilator couples to fabricate green and yellow upconversion luminescent emissive nanocapsules, named UCNC-G and UCNC-Y, respectively. In water under the atmospheric environment, interestingly, UCNC-G and UCNC-Y exhibit intense upconversion luminescence (UCL) emission (λ_{ex} = 635 nm) with the quantum efficiencies (Φ_{UCL}) of 1.7% and 4.8%, respectively, whereas very weak UCL emission (Φ_{UCL} < 0.1%) was observed for the corresponding previous reported SiO_2-coating nanosystems because of aggregation-induced fluorescence quenching of annihilators. Furthermore, application of theses upconversion nanocapsules for high-contrast UCL bioimaging *in vivo* of living mice without removing the skin was demonstrated under 635-nm excitation with low power density of 12.5 mW cm^{-2}.
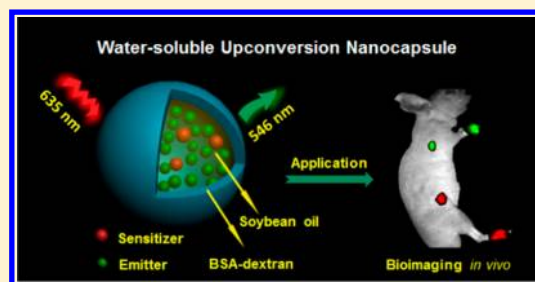
■ INTRODUCTION

Upconversion luminescence (UCL) is a unique process in which low-energy photons are converted into high-energy ones.[1−3] Triplet−triplet annihilation (TTA)-based upconversion luminescence (TTA-UCL), involving the transfer of energy between sensitizer and annihilator and triplet−triplet annihilation among two annihilator molecules, has emerged as an efficient upconversion process.[1,3] TTA-UCL process has some advantages including the adjustable excitation and emission wavelength by independent selection of sensitizer and annihilator, intense absorption coefficient of the sensitizer ($\sim 10^{-17}$ cm^2), and high quantum efficiency (even $\sim$20% in organic solvent).[4] Unfortunately, most of the reported TTA-based upconversion systems have been fabricated in organic solution, such as toluene, chloroform, and so on, which limit their wide application in bioimaging. Recently, SiO_2 coating[5] and polymer enclosing[6] strategies have successfully been developed to synthesize water-soluble nanoparticles with blue TTA-UCL emission. In these two methods, organic solvents were almost excluded and aggregation-induced luminescence quenching will become problematic when rigid planar or polar structure is adopted for long-wavelength annihilators (such as BODIPY dyes[7]). As a result, no example of green/red water-soluble upconversion nanoparticle based on TTA process has

been reported to date. Therefore, a general strategy of integrating the sensitizer and annihilator into one water-soluble nanoparticle to avoid aggregation-induced luminescence quenching is necessary.
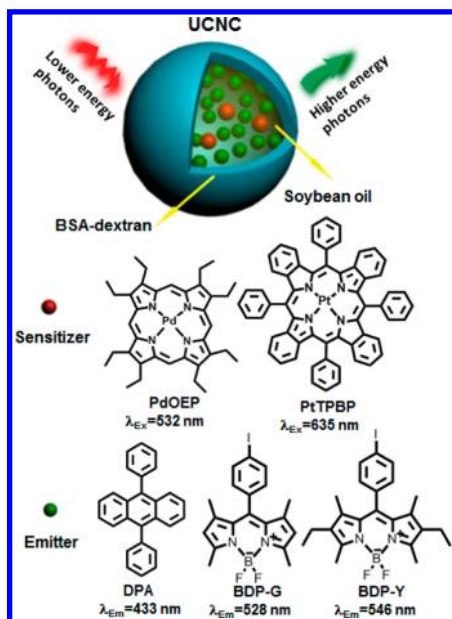
Obviously, it becomes a key point to keep the organic solvent in the as-prepared water-soluble nanoparticles to achieve high efficiency UCL, by maintaining high translational mobility[8] of the chromophores and avoiding luminescence quenching by aggregation. In the present study, we developed a general method of nanocapsule (Scheme 1) by integrating the sensitizer and annihilator into an emulsion nanosystem with nanosized oil-in-water droplet to fabricate water-soluble TTA-based upconversion system with effective green or yellow TTA-UCL emission.[9]

Our design strategy was to fabricate nanosized oil droplets with stable bovine serum albumin (BSA) film at the oil−water interface and hydrophilic dextran on the droplet surface (Scheme S1). Soybean oil approved by FDA as an injectable component was chosen as oil phase, in which the sensitizer/annihilator couples can keep excellent solubility and show intense photoluminescence emission. BSA has a strong

Scheme 1. Schematic Illustration of TTA-UCL Process of the Upconversion Nanocapsules (UCNC), and Chemical Structures of Sensitizers (PdOEP and PtTPBP) and Annihilators (DPA, BDP-G, and BDP-Y)

■ RESULT AND DISCUSSION

Upconversion Luminescence Properties in SiO₂ Nanoparticles. It is noteworthy that these previously reported upconversion systems PtTPBP/BDP-G and PtTPBP/BDP-Y,[9] when capped in SiO₂ nanoparticles using our previously reported strategy,[5] were ineffective (Figure 1a), and only
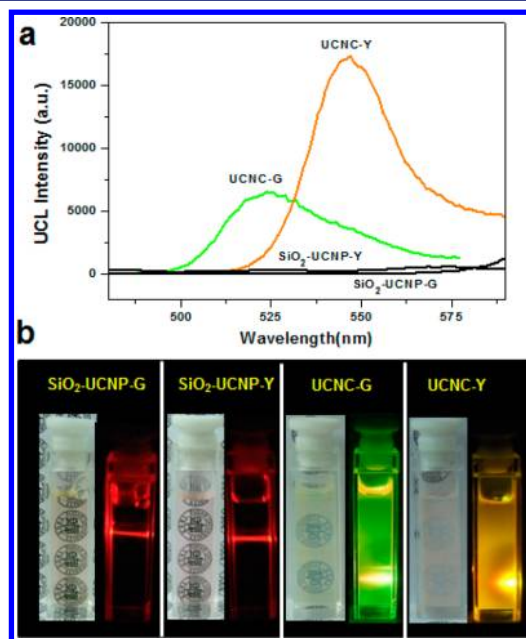

Figure 1. (a) Upconversion luminescence (UCL) emission spectra of the SiO₂-UCNP-G, SiO₂-UCNP-Y, UCNC-G, and UCNC-Y dispersed in water, under excitation at 635 nm. The concentrations of the sensitizer (PtTPBP) and annihilator (BDP-G or BDP-Y) in these nanosystems are fixed to be 5.0×10^{-7} and 5.0×10^{-5} mol L^{-1}, respectively. (b) The photos of bright-field and UCL emission of SiO₂-UCNP-G, SiO₂-UCNP-Y, UCNC-G, and UCNC-Y in water inside the 1×10 mm cuvette. The UCL emission images were achieved with a camera equipped with a short-pass filter of 635 nm. The red shown in panels b is excited 635 nm laser.

tendency to absorb at the oil−water interface to lower the surface tension.[10] BSA, similar to human serum albumin (HSA), contains tryptophan to react with singlet oxygen that usually quench UCL emission, and therefore benefits UCL emission. Dextran can enhance the hydrophility of the droplet surface and provide steric repulsion of the oil droplet, protecting the droplet from coalescence and flocculation.[11] In addition, in these oil-in-water nanocapsules, a heat treatment was carried out to cause the BSA denaturation, forming stable oil−water interfacial film.[12] Therefore, BSA-dextran conjugate, produced via a naturally occurring Maillard reaction between the ε-amino group in BSA and the reducing-end carbonyl group in dextran,[13] was herein used as emulsifier and stabilizer.

To show the validity of this emulsion nanometer oil-in-water droplet, herein, the BODIPY dyes (BDP-G and BDP-Y,[9] Scheme 1) which have significant aggregation-induced quenching of fluorescent emission[7] were chosen as the annihilators. Pt(II)-tetraphenyl-tetrabenzoporphyrin (PtTPBP, Scheme 1) was used as the sensitizer. Interestingly, the as-prepared oil-in-water nanocapsules with PtTPBP/BDP-G and PtTPBP/BDP-Y as sensitizer/annihilator couples (named UCNC-G and UCNC-Y, respectively, in Scheme 1) exhibit intense UCL emission (λ_{ex} = 635 nm) with quantum efficiency (Φ_{UCL}) of 1.7% and 4.8% in water under the atmospheric environment. On the contrary, using the our previous SiO₂ coating method,[5] the obtained nanoparticles showed very weak UCL emission (Φ_{UCL} < 0.1%, λ_{ex} = 635 nm). Furthermore, these green and yellow-emissive nanocapsules were for the first time used for *in vivo* UCL imaging of the lymph nodes in whole-body small animals without skin removal under low power density excitation at 635 nm (12.5 mW cm^{-2}). To confirm the generality of this strategy, another sensitizer/ annihilator couple of PdOEP/DPA (Scheme 1) was adopted to prepare effective, blue-emissive upconversion nanocapsules, named UCNC-B, with Φ_{UCL} of 6.2%.

excitation laser at 635 nm was observed (Figure 1b). Herein, the SiO₂ nanoparticles enclosed with PtTPBP/BDP-G and PtTPBP/BDP-Y were abbreviated as SiO₂-UCNP-G and SiO₂-UCNP-Y, respectively. The upconversion quantum efficiency (Φ_{UCL}) values of <0.1% were measured for SiO₂-UCNP-G and SiO₂-UCNP-Y (Table 1).

It is well-known that, during the upconversion luminescence process (Scheme S2), the electron in a single excited state transits to the ground state, with the emission of luminescence by the emitter.[1b] The fluorescence quantum yield (Φ_{FL}) of the emitter is thus an important factor affecting upconversion quantum efficiency. Generally, BODIPY dyes show significant aggregation-induced luminescence quenching. As shown in Figure S1, the powder of BDP-G and BDP-Y displayed very weak fluorescence emission under excitation at 365 nm, which is different from that of blue emissive DPA. Moreover, the fluorescence properties under 365-nm excitation of SiO₂-UCNP-Y (as an example) were also investigated. As shown in Figure S2, obviously fluorescent quenching of BDP-Y in SiO₂ nanoparticles can be observed, which therefore cause weak UCL emission of SiO₂-UCNP-G and SiO₂-UCNP-Y. Thus, it is necessary to develop new synthetic strategy to fabricate effective water-soluble upconversion nanoparticles.

Table 1. Upconversion Luminescence Quantum Efficiencies (Φ_{UCL}) for the Different Systems (Including Toluene Solution, Soybean Oil Solution, Nanocapsule, SiO$_2$ Nanoparticles) Containing PtTPBP/BDP-G and PtTPBP/BDP-Y under Excitation at 635 nm[a]

| | Φ_{UCL} | | | | | |
| | condition | | | | | |
system	in toluene[b]	in toluene[c]	in soybean oil[b]	in soybean oil[c]	in nanocapsules[b]	SiO$_2$-coating[b]
PtTPBP/BDP-G	0.2%	7.6%(6.2%)[9]	2.4%	2.5%	1.7%	<0.1%
PtTPBP/BDP-Y	0.1%	14.3%(15.0%)[9]	5.0%	5.0%	4.8%	<0.1%

[a]Methyl blue in methanol was chosen as a reference.[9] The concentrations of sensitizer and annihilator in soybean oil, toluene and SiO$_2$-coating system are 1.0×10^{-5} and 1.0×10^{-3} mol L^{-1}, respectively. In nanocapsule, the concentrations of the sensitizer and the annihilator are 1.0×10^{-5} and 1.0×10^{-3} mol L^{-1} relative to soybean oil, and are 5.0×10^{-7} mol L^{-1} and 5.0×10^{-5} mol L^{-1} relative to water. The excitation power density at 635 nm is 106 mW cm^{-2}. [b]Under aerated conditions with the presence of oxygen. [c]Under a positive argon environment and in the absence of oxygen.

Upconversion Luminescence Properties in Soybean Oil.

Before preparing upconversion nanocapsules with the soybeal oil as the core, the UCL properties of the PtTPBP/BDP-G and PtTPBP/BDP-Y solution in soybean oil were investigated. As shown in Figure 2, intensive green and yellow
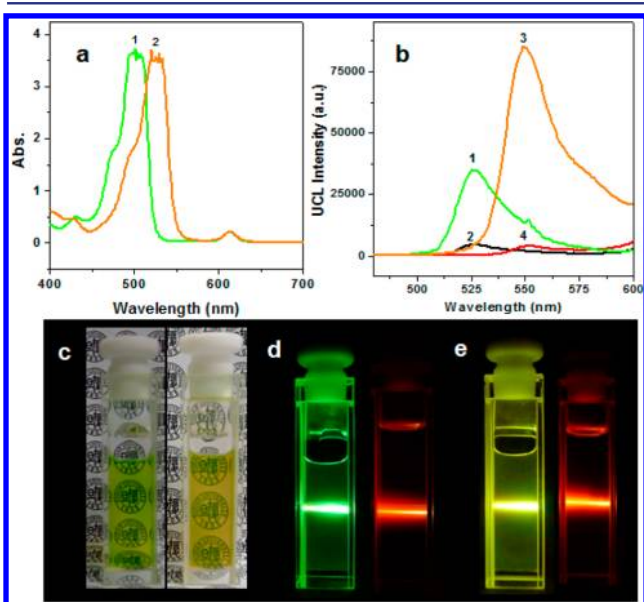

Figure 2. (a) The absorption spectra of PtTPBP/BDP-G (green, 1) and PtTPBP/BDP-Y (orange, 2) in soybean oil. (b) UCL emission spectra of PtTPBP/BDP-G in soybean oil (green, 1) and in toluene (black, 2) and PtTPBP/BDP-Y in soybean oil (orange, 3) and in toluene (red, 4). (c) The bright-field photos of PtTPBP/BDP-G (left) and PtTPBP/BDP-Y (right) in soybean oil. (d) UCL emission photos of PtTPBP/BDP-G in soybean oil (left) and toluene (right), (e) UCL emission photos of PtTPBP/BDP-Y in soybean oil (left) and toluene (right). All the measurements were carried out in the presence of oxygen, with a short-pass filter of 635 nm. The concentrations of sensitizer (PtTPBP) and the annihilator (BDP-G or BDP-Y) are 1.0×10^{-5} and 1.0×10^{-3} mol L^{-1}, respectively.

UCL emissions were observed for PtTPBP/BDP-G and PtTPBP/BDP-Y in soybean oil in the presence of oxygen, with the Φ_{UCL} of 2.4% and 5.0% (Table 1), respectively. In contrast, weakly UCL signals were detected when these two sensitizer and annihilator couples were dissolved in toluene under the aerated conditions, with the Φ_{UCL} of 0.2% and 0.1% (Table 1). Such significant enhancement of Φ_{UCL} in soybean oil system in comparison with toluene system illustrated that the

soybean oil can served as an excellent solvent for high-efficient UCL emission under the presence of oxygen.

Considering that the fluorescence quantum yield (Φ_{FL}) of the annihilator affects upconversion quantum efficiency significantly, we further investigated the Φ_{FL} of BDP-G (as an example annihilator) in toluene and soybean oil. The Φ_{FL} of BDP-G in soybean oil was 79%, which was higher than that (Φ_{FL} = 59%) in toluene. It is possible that the high viscosity of soybean oil decreases free rotation of the phenyl group, thus reducing loss of energy from the excited states via non-irradiative molecular motion. However, such 1.3-fold increase in the Φ_{FL} of BDP-G cannot explain the considerable enhancement (~12-fold) of UCL emission in soybean oil.

In the TTA-based upconversion process, oxygen-induced UCL quenching is usually a serious issue under atmospheric environment, because the triplet energy of the sensitizer can also be transferred to oxygen and singlet oxygen is formed.[1b] We therefore investigated the UCL properties of PtTPBP/BDP-G and PtTPBP/BDP-Y in soybean oil in the presence and absence of oxygen. As shown in Table 1, no significant changes in UCL emission were observed for PtTPBP/BDP-G or PtTPBP/BDP-Y in soybean oil in the presence or absence of oxygen, which differed from the case in toluene. This lack of significant oxygen-induced UCL quenching in soybean oil is reported for the first time.

The main components of soybean oil are linoleic acid (LA) and oleic acid (OA), both of which show reducing ability. It is therefore possible that the generated singlet oxygen in our upconversion system may be consumed in the reducing environment, decreasing the concentration of oxygen, and benefiting the TTA-UCL emission. To confirm this hypothesis, the nontoxic nutritional antioxidant preservative ascorbyl palmitate was used as a reducing agent and added into the toluene solution with BDP-G (1.0×10^{-3} mol L^{-1}) and PtTPBP (1.0×10^{-5} mol L^{-1}). The UCL emission intensity was enhanced with increasing concentrations of ascorbyl palmitate (Figure S3). At a low concentration of 2.0×10^{-3} mol L^{-1}, the UCL intensity was increased with prolonged exposure time at 635-nm illumination (106 mW cm^{-2}). However, no significant change in the UCL intensity of PtTPBP/BDP-G in toluene was observed after 635-nm irradiation for 180 s, indicating that a balance between oxygen diffusion and consumption has been achieved. In the presence of a higher concentration of ascorbyl palmitate (5.0×10^{-3} mol L^{-1}), no significant increase in the UCL intensity was measured with prolonged exposure to a 635-nm laser within 30 min (Figure S3), suggesting that the rapid balance between oxygen diffusion and consumption was achieved in comparison of the

case with low concentration of ascorbyl palmitate. These results suggest that soybean oil may affect UCL emission similar to the reducing agent ascorbyl palmitate.

We also investigated the effect of a reducing environment on the phosphorescent lifetime of PtTPBP. The phosphorescent lifetime of PtTPBP in toluene with prolonged exposure to 635-nm laser for 240 s was increased to ∼32 μs (Figure S4) in the presence of ascorbyl palmitate (2.0 × 10^{-3} mol L^{-1}). Interestingly, after 635-nm irradiation for 30 s, the phosphorescent lifetime of PtTPBP in soybean oil in the presence of oxygen was ∼39 μs, which was similar to that (40 μs) of PtTPBP in toluene under an argon environment. In addition, the nanosecond time-resolved transient difference absorption spectrum of PtTPBP in soybean oil was measured. As shown in Figure S5, the lifetime of the triplet excited state of PtTPBP in soybean oil was prolonged from 2.4 to 27 μs, after 635-nm irradiation for 30 s. These results indicate high level of reducing agents in soybean oil has an important positive effect on the phosphorescent lifetime and triplet energy level of the sensitizer (PtTPBP).

The UCL lifetimes of PtTPBP/BDP-G in different environments (soybean oil, or toluene in the absence or presence of ascorbyl palmitate) were also determined. The UCL lifetime in toluene was relatively short (<1.0 μs, Figure 3a), but was prolonged in the presence of ascorbyl palmitate from 5 to 40 μs when the 635-nm irradiation time was increased from 120 to 240 s (Figure 3b), respectively. Interestingly, as shown in the

video in the Supporting Information, when the 635 nm laser was moved, a flickering UCL emission was observed, indicating that the oxygen consumption in soybean oil was rapid and that oxygen diffusion was slow under irradiation with a 635-nm laser. As a result, the UCL lifetime in soybean oil could reach 81 μs without preirradiation by a 635-nm laser (Figure 3a), indicating that soybean oil represents an excellent medium for highly effective TTA-UCL emission.

In addition, linoleic acid (LA) and oleic acid (OA) of high purity (>99%) were used as solvents for PtTPBP/BDP-G. As shown in Figure S6, PtTPBP/BDP-G in either OA or LA showed intense UCL emission with high Φ_{UCL} values of 1.6% and 1.7%, respectively, which were similar to the Φ_{UCL} in soybean oil. This suggests that both OA and LA in soybean oil play crucial roles in TTA-based UCL.

These results indicate that soybean oil can act as an excellent solvent for highly effective TTA-based UCL emission because of the high effective oxygen consumption in this solvent. In addition, soybean oil has been approved by FDA as an injectable component. The present study therefore used soybean oil as the medium for fabricating water-soluble nanocapsule.

Nanocapsules Characterization. The upconversion nanocapsules loaded with sensitizer and annihilator were characterized by transmission electron microscopy (TEM), dynamic light scattering (DLS) and ζ-potentials analysis.

Figure 4a shows a TEM image of UCNC-G. The homogeneous UCNC-G presents polygonal shapes due to
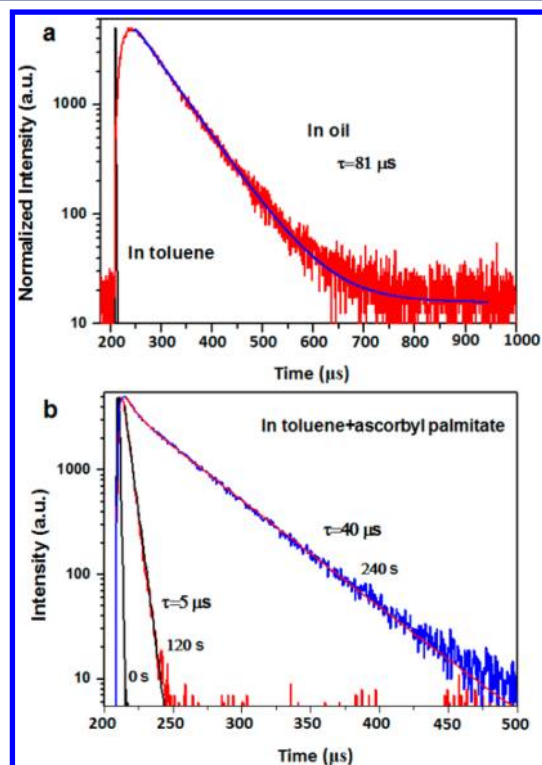

Figure 3. (a) Delayed luminescence observed in the TTA upconversion of PtTPBP/BDP-G in soybean oil (red line) or in toluene (black line) with the presence of oxygen (λ_{ex} = 635 nm, λ_{em} = 528 nm). (b) Delayed luminescence observed in the TTA upconversion of PtTPBP/BDP-G in toluene, which contains ascorbyl palmitate (2.0 × 10^{-3} mol L^{-1}), under exposure of 635-nm laser with different times (0, 120, and 240 s) (106 mW cm^{-2}, λ_{ex} = 635 nm, λ_{em} = 528 nm).
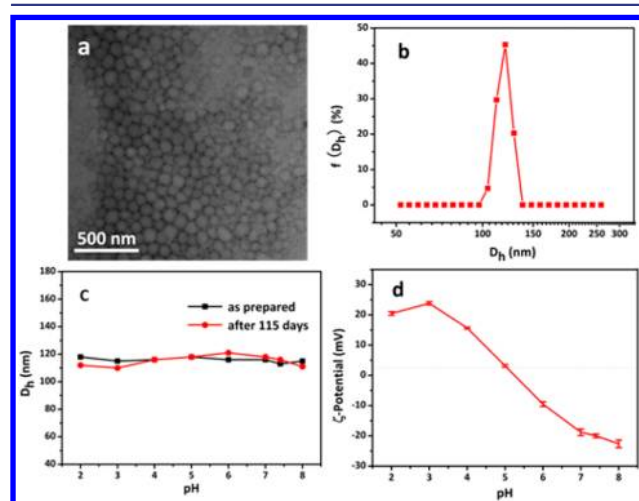

Figure 4. (a) Transmission electron microscopy and (b) size distribution of UCNC-G in pure water. (c) The nanocapsules size of UCNC-G before and after 115 days of the storage in different pH media, and (d) ζ-potential of UCNC-G as a function of pH.

their soft and deformable nature of the nanocapsules. Figure 4b presents the size distribution of UCNC-G obtained by DLS. The z-average hydrodynamic diameter (D_h) is 116 nm. The size distributions of UCNC-B and UCNC-Y are shown in Figure S7 (Supporting Information), with D_h of 93 and 95 nm, respectively. The stability of UCNC-G against the changes of pH as well as long-term storage in different media was investigated. As shown in Figure 4c, no significant change in the nanocapsule size was observed in the pH range of 2−8 even after 115 days of the storage, which is attributed to the stable BSA film at the oil−water interface and the hydrophilic dextran on the nanocapsule surface. Furthermore, the size remains

unchanged after 4 months of the storage in the medium of pH 7.4 containing 0.2 mol L^{-1} NaCl. This result indicates that the nanocapsules are stable in physiological condition and applicable in bioimaging *in vivo*. Figure 4d shows the ζ-potential of UCNC-G as a function of pH. UCNC-G carries positive charges and negative charges when the pH is lower and higher than 5.2, respectively. At physiological pH 7.4, the ζ-potential value is -19.7 mV, which is suitable for bioapplication.[14]

The successful loading of the sensitizer and annihilator into the BSA−dextran emulsion nanocapsules was confirmed by absorption spectroscopy. In the absorption spectrum of UCNC-G (Figure S8), the appearance of the characteristic bands of both PtTPBP (at 610 nm) and BDP-G (at 504 nm) confirmed the coexistence of PtTPBP and BDP-G in the UCNC-G. Similarly, the absorption bands of both PtTPBP/BDP-Y were observed for UCNC-Y. Moreover, as determined by absorption spectroscopy, extraction of these upconversion nanocapsules systems yielded less than 1% of uploaded sensitizer and annihilator, indicating that the loading proportions of sensitizer and annihilator in the nanocapsules can reach to almost quantitative.

Upconversion Luminescence Properties of Nanocapsules. Before investigating the upconversion properties of nanocapsules, we first studied the annihilator concentration-dependence of the UCL property of PtTPBP/BDP-G in toluene. As shown in Figure S9, the UCL emission first increased, and then became weaker as the concentration of annihilator BDP-G increased. The UCL peak show red-shifting from 530 to 550 nm, which also indicated that aggregation is more and more significant in the presence of higher concentration of BDP-G (Figure S10). With selective excitation at 635 nm, the photoluminescence spectra of UCNC-G and UCNC-Y in aqueous solutions were shown in Figure 1a and Figure S11. For these two systems, both phosphorescent emission of PtTPBP and significant UCL emission with a center band at 528 nm (for BDP-G) or 546 nm (for BDP-Y) were observed, which further confirmed the coexistence of sensitizer (PtTPBP) and annihilator (BDP-G or BDP-Y) in a single nanocapsule. The green or yellow UCL emission was visible to the naked eye for the UCNC-G or UCNC-Y (Figure 1b), respectively, which coincides with previous observations of PtTPBP/BDP-G and PtTPBP/BDP-Y in organic solution.[8] Moreover, as shown in Figure 1, the UCNC-G and UCNC-Y display significantly brighter UCL emission than those in the corresponding SiO$_2$ nanoparticles. Therefore, using this strategy of BSA−dextran coated oil nanocapsule, high efficiency of green and yellow UCL emission based on triplet−triplet annihilation process in water has been observed. The UCL blue emission also can be observed from UCNC-B (Figure S12 and S13), which further confirmed the generality of this strategy.

Furthermore, the integrated UCL intensity of UCNC-G and UCNC-Y were enhanced as the incident laser power increased (Figure 5a,b). The quadratic dependence of the UCL emission intensity on laser power density is demonstrated in the range of lower power density. In higher power density, however, the UCL emission intensity showed a linear dependence. The above-mentioned relationship between UCL emission intensity and excitation power density is in agreement with the previous observation.[3i]

To further confirm that the UCL emission is from the TTA-based upconversion, the delayed UCL kinetics was investigated. The lifetime of the upconversion green emission of UCNC-G
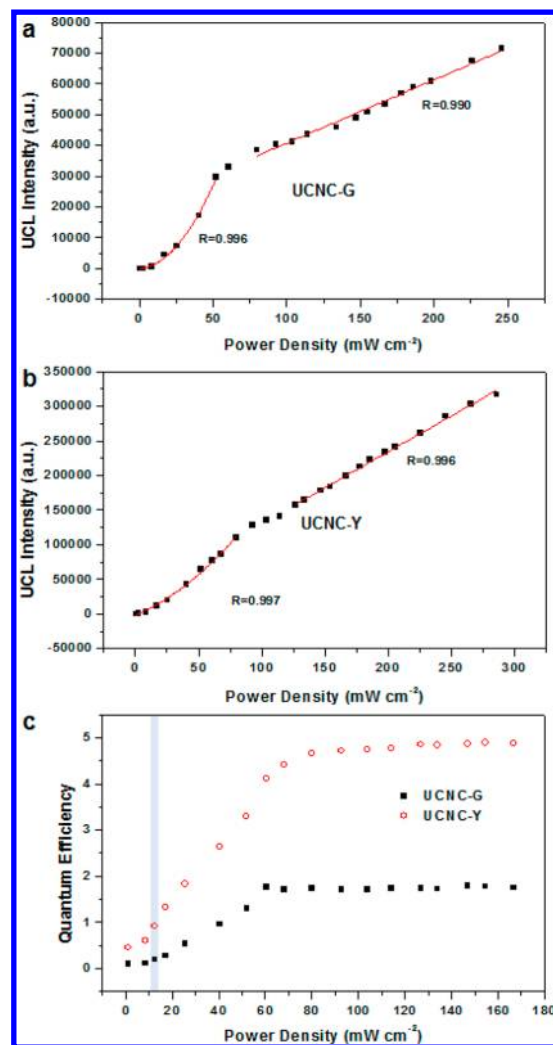

Figure 5. (a and b) The dependence of UCL emission intensity on excitation power density of UCNC-G (a) and UCNC-Y (b), the solid lines are the fits with quadratic and liner response in the low and high power density regimes, respectively. (c) Upconversion quantum efficiency of UCNC-G (black dots) and UCNC-Y (red dots) measured as a function of incident light power density. The concentrations of the sensitizer PtTPBP and the annihilator (BDP-G or BDP-Y) are 5.0×10^{-7} and 5.0×10^{-5} mol L^{-1}, respectively. The shadow in panel c shows the UCL quantum efficiency under the excitation power density of 12.5 mW cm^{-2}.

was determined to be 71.3 μs (Figure 6a), significantly longer than the fluorescence lifetime (6.1 ns) of BDP-G under excitation at 397 nm (Figure 6b). Such an exceptionally long-lived luminescence emission confirms that the green emission is related to the TTA-based upconversion process, involving a long-lived triplet state. Compared with the TTA-UCL lifetime (81 μs, Figure 3a) of the soybean oil system containing PtTPBP as sensitizer and BDP-G as annihilator, no significant decrease in TTA-UCL lifetime was observed for UCNC-G in aqueous solution, indicating that the TTA-UCL emission could be generated in this nanocapsule efficiently.

It is well-known that the UCL quantum efficiency (Φ_{UCL}) is dependent on the measured conditions, including the excitation power density, concentrations of the sensitizer and annihilator, solvent polarity, and oxygen concentration. In particular, the presence of oxygen has a large negative effect on the UCL quantum effciency.[15] However, in light of the fact that the
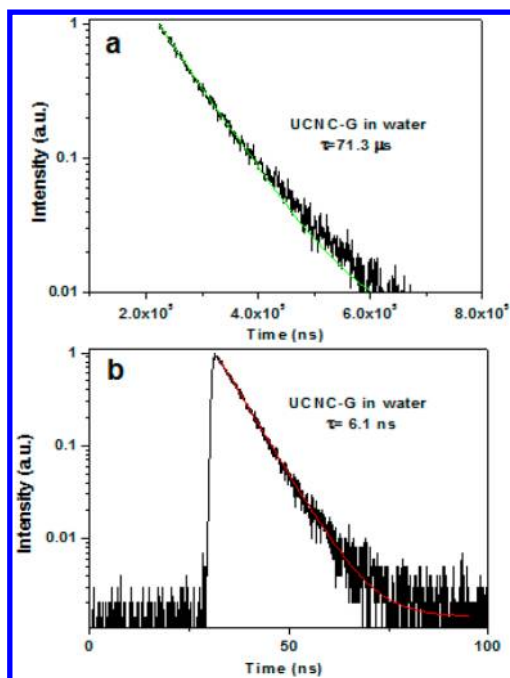
Figure 6. (a) Delayed luminescence observed in the TTA upconversion of UCNC-G in water in the presence of oxygen (λ_{ex} = 635 nm, λ_{UCL} = 528 nm). (b) Prompt fluorescence lifetime of UCNC-G in water in the presence of oxygen (λ_{ex} = 397 nm, λ_{em} = 528 nm).

presence of oxygen is inevitable during bioimaging applications, the Φ_{UCL} of the upconversion systems were investigated in an atmosphere containing oxygen. With methylene blue as a reference,[16] we have measured the effect of power density to the Φ_{UCL} in water under the presence of oxygen. As shown in Figure 5c, first as the power density increased, the quantum efficiencies were increased to 1.7% and 4.8% for UCNC-G and UCNC-Y, respectively. After the excitation power density was increased to ~60 or ~80 mW cm^{-2} for UCNC-G and UCNC-Y, respectively, no significant change in the Φ_{UCL} was observed. The Φ_{UCL} of UCNC-G and UCNC-Y in water is similar to the result in soybean oil of 2.4% and 5.0% (Table 1), respectively. It should be noted that the Φ_{UCL} based on triplet−triplet annihilation is significantly higher than those of lanthanide-doping upconversion nanophosphors,[1,2] although the Φ_{UCL} value of UCNC-G and UCNC-Y was measured in water.

Moreover, it should be noted that this nanocapsule-loading method is a general strategy of fabricating high efficient upconversion nanomaterial with or without aggregation-induced fluorescence quenching of the annihilators. For example, using this soybean oil based nanocapsule strategy, another sensitizer/annihilator couple of PdOEP/DPA (Scheme 1) was adopted, and effective, blue-emissive upconversion nanocapsule (UCNC-B) was also prepared (Figure S13). The Φ_{UCL} of the UCNC-B was determined, up to 6.2%, which is higher than that of the corresponding silica nanoparticles (Φ_{UCL} = 4.5%).[5] In the nanocapsules, soybean oil acts as a hydrophobic solvent preserving the high translational mobility of the chromophores (sensitizer and annihilator) and avoiding quenching by aggregation, and is also used as reducing agents to achieve the oxygen consumption. Therefore, the nanocapsule's special structure of BSA−dextran coating soybean oil promoted a highly effective UCL process in water medium.

Photostability of the Nanocapsule UCNC-G. Moreover, possible photobleaching of the TTA-UCNC system was considered. No significant change in the UCL emission was observed when UCNC-G was continuously irradiated by a CW 635-nm laser (106 mW cm^{-2}) for about 1 h (Figure S14), suggesting excellent photostability for UCNC-G. In addition, the upconversion nanocapsule system was quite stable for more than 115 days of exposure to the atmosphere.

Penetration Depth in UCL Imaging. In addition, we compared the abilities of UCNC-B, UCNC-G and UCNC-Y to penetrate tissue by covering upconversion nanocapsules with beef slices. In the UCL imaging without beef slices, the UCNC-B displays much brighter UCL signal than UCNC-G and UCNC-Y do, as shown in Figure 7, However, when covered
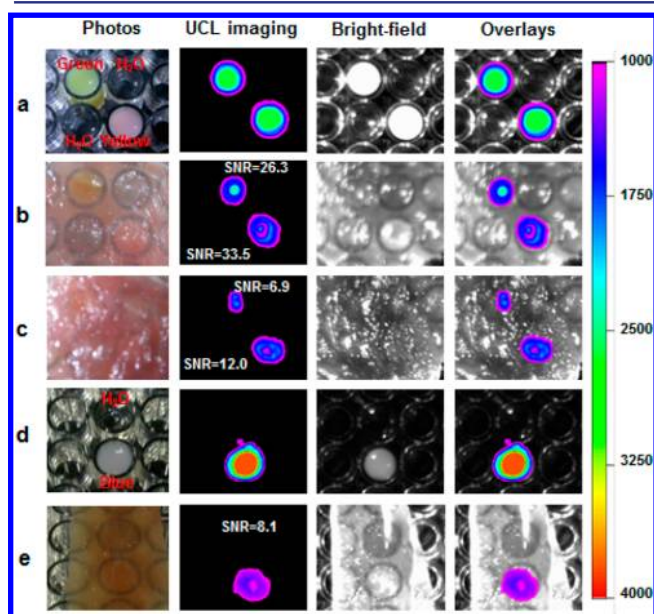

Figure 7. (a−c) Penetration depth experiment of UCNC-G (green) and UCNC-Y (yellow) without beef slice (a), with 0.1 cm beef slice (b) and with 0.2 cm beef slice (c) (λ_{ex} = 635 nm, λ_{UCL} = 530 ± 25 nm, excitation power density of 12.5 mW cm^{-2}). (d and e) Penetration depth experiments of UCNC-B (blue) without beef slice (d) and with 0.1 cm beef slice (e) (λ_{ex} = 532 nm, λ_{UCL} = 452 ± 25 nm, excitation power density of 13 mW cm^{-2}). Water was used as the control sample in this penetration depth experiment.

with a 0.1 cm beef slice (Figure S15), the UCL signal from UCNC-B (Figure 7e) decreased remarkably compared with the cases of UCNC-G and UCNC-Y (Figure 7b), and then the signal-to-noise ratio (SNR = 8.1) of UCNC-B is significantly lower than those of UCNC-G and UCNC-Y, which is attributed to the low penetration depth of the blue emission. The penetration abilities of UCNC-G and UCNC-Y were further investigated when covering with a 0.2 cm beef slice. Clear UCL signals could be observed for UCNC-G and UCNC-Y with signal-to-noise ratios of 6.9 and 12.0 (Figure 7c), respectively. These results indicated that UCNC-G and UCNC-Y provide better penetration ability than UCNC-B.

***In Vivo* and *ex Vivo* UCL Imaging.** Upconversion luminescence via sensitized triplet−triplet annihilation is a nonlinear process and the excitation energy will have a big effect in the upconversion efficiency. Herein, UCL bioimaging *in vivo* of living mouse with subcutaneous-injection of UCNC-G (20 µL) were carried out under different excitation power densities (Figure 8). The signal-to-noise ratio (SNR) value in UCL imaging was increased as the excitation power density
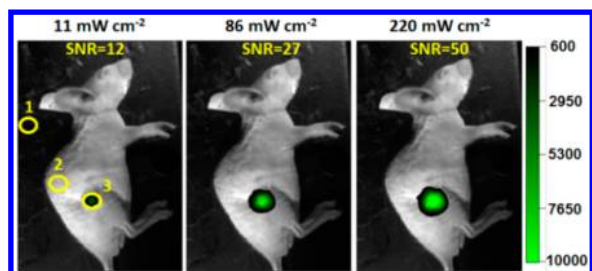
Figure 8. *In vivo* upconversion luminescence imaging of the living mouse with subcutaneous injection of 20 μL UCNC-G under different excitation power density of 11, 86, and 220 mW cm^{-2}, (λ_{ex} = 635 nm, λ_{UCL} = 530 $\pm$ 25 nm). Signal-to-noise ratio (SNR) = [(mean luminescence intensity of signal region 3) − (mean luminescence intensity of background region 1)]/[(mean luminescence intensity of the noise region 2) − (mean luminescence intensity of background region 1)].

increased. It should be noted that, in biosamples, the process of upconversion luminescence emission is completely absent and there is no background from autofluorescence. Bioimaging *in vivo* can thus maintain a high SNR of 12, even at a low excitation power density (11 mW cm^{-2}).

In light of the deeper penetration depth achievable using UCNC-G and UCNC-Y as bioimaging probes compared to blue UCL emissive UCNC-B, lymphatic imaging *in vivo* of small animals without removing their skin was carried out. UCNC-G and UCNC-Y were injected intradermally into the foreclaw and hindclaw, respectively. Upon low-power density excitation with a CW 635-nm laser (12.5 mW cm^{-2}), clear signals (using a band-pass filter of λ_{em} = 530 $\pm$ 25 nm) were detected in the lymphatic drainage basins of the oxter without removing the skin, with an excellent signal-to-noise ratio (∼13 for UCNC-G and 18 for UCNC-Y) (Figure 9a). Imaging *in situ* and *ex vivo* further confirmed the UCL signals were from the lymph nodes of the oxter (Figure 9b,c). That detected signal was from the emission of TTA-based UCL was confirmed by measuring the spectrum *in vivo* utilizing a fiber optic spectrometer (PG2000Pro, Ideaoptics Co., China). As shown in Figure 9d, significant TTA-UCL emission peaking at 522 and 546 nm can be observed, which is almost in agreement with the above-mentioned spectral data (Figure 1). As shown in Figure 9e, hematoxylin and eosin (H&E)-stained sections further supported that the biosample which can be selectively excited with a 635-nm laser and generate UCL emission is lymph node.

CONCLUSION

In summary, we demonstrated an excellent solvent of soybean oil for highly effective triplet−triplet annihilation-based upconversion luminescence (TTA-UCL) emission in solution phase and a general strategy for constructing biocompatible upconversion nanocapsules in water phase. Water-soluble nanocapsules exhibiting TTA-UCL emission were successfully prepared by loading sensitizer and annihilator into BSA−dextran stabilized oil droplets, which act as solvent for dissolving the sensitizer and annihilator. This strategy can maintain high translational mobility of the chromophores, avoid quenching by aggregation, and decrease the O$_2$-induced TTA-UCL quenching, to produce high efficient UCL emission. The UCL quantum efficiency of UCNC-G and UCNC-Y can be as high as 1.7% and 4.8%, respectively, even under the atmospheric environment in water. In particular, these upconversion nanocapsules were successfully applied to
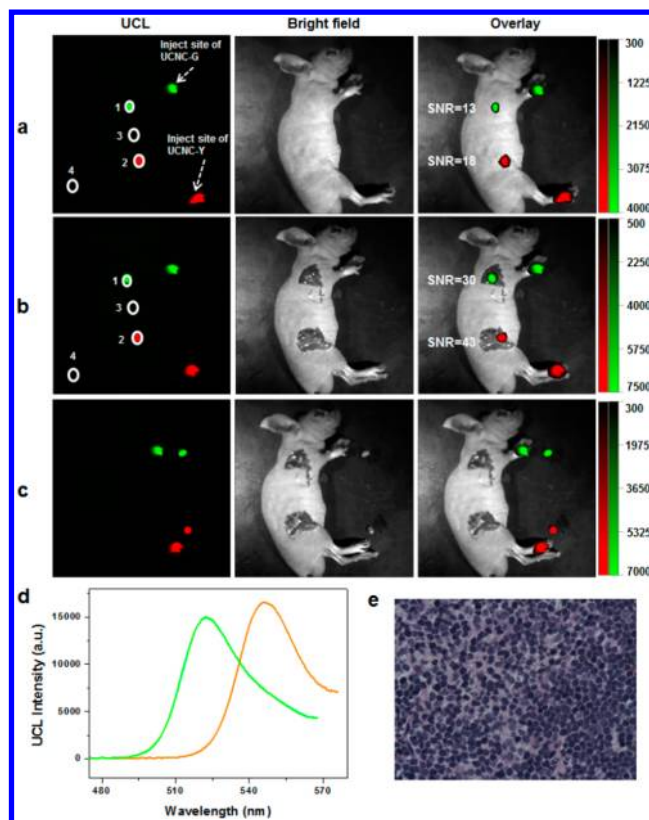

Figure 9. (a) *In vivo*, (b) *in situ* and (c) *ex vivo* upconversion luminescence lymphatic imaging of the living mouse at 30 min postinjection of 20 μL UCNC-G and UCNC-Y in forepaw and hindpaw, respectively (λ_{ex} = 635 nm, λ_{UCL} = 530 $\pm$ 25 nm, excitation power density of 12.5 mW cm^{-2}). (d) UCL spectra of UCNC-G and UCNC-Y in lymph nodes. (e) H&E-stained section of lymph node from the mouse injected with UCNC-G for 30 min. SNR stands for signal-to-noise ratio.

lymph node imaging *in vivo* of living mice without removing the skin, achieving excellent signal-to-noise ratios (>10), upon low-power density excitation by a CW laser (12.5 mW cm^{-2}). The present observation of the high effective oxygen consumption in the presence of reducing agents (such as soybeal oil) will provide a new applied field in sensing and bioimaging. This study opens up new perspectives for integrating TTA-based UCL materials and application in bioimaging *in vivo*.

EXPERIMENTAL SECTION

Materials. All reagents and solvents were used as received without further purification: Pd complex octaethylporphyrin (PdOEP), 9,10-diphenylanthracene (DPA), and rhodamine B were purchased from Aldrich. Pt-tetraphenyltetrabenzoporphyrin (PtTPBP) was purchased from Luminescence Technology Crop. BSA (fraction V, 99%) and dextran (molecular weight 10 kDa) were purchased from AMRESCO, Inc. Reagent grade toluene and methylene blue were purchased from Sinopharm Chemical Reagent Co., Ltd. Soybean oil for injection was from Jiangxi Golden Crabapple Medicinal Oil Co. Ltd. BDP-G and BDP-Y were synthesized according to published procedures. Deionized water was used in the experiments throughout.

Preparation of Sensitizer and Annihilator (PdOEP/DPA, PtTPBP/BDP-G, and PtTPBP/BDP-Y) Encapsulated BSA−dextran Nanocapsules. BSA−dextran conjugate was prepared by Maillard reaction as reported previously.[17] In this study, 10 kDa dextran was used to prepare BSA−dextran conjugate in which the molar ratio of BSA to dextran was 1:6. The BSA−dextran conjugate

was dissolved in deionized water with BSA concentration of 10.0 mg mL^{-1}. Sensitizer and annihilator with 1:100 molar ratio were dissolved together in a mixed oil phase composed of soybean oil and toluene (1:1, v/v), in which the annihilator concentration was 1.0 mmol L^{-1}. The mixed oil phase was added into the conjugate aqueous solution with 10% oil volume fraction. The mixture was pre-emulsified at room temperature using a homogenizer (FJ200-S, Shanghai Specimen Model Co.) at 10 000 rpm for 1 min, and then was immediately emulsified using a high pressure homogenizer (AH100D, ATS Engineering, Inc.) at 850 bar for 4 min. The emulsion was heated at 90 °C for 1 h. The toluene and water in the emulsion were removed under reduced pressure at 40 °C. Then, the droplets were dispersed in water and the resultant emulsion was filtrated with 0.8 μm membrane to obtain sterile emulsion.

Synthesis of SiO$_2$-Coated PdOEP/DPA, PtTPBP/BDP-G and PtTPBP/BDP-Y Nanoparticles. The nanoparticles were synthesized according to a previously reported procedure.[5] In a 20 mL glass scintillation vial, 200 mg of Pluronic F127, 2.0×10^{-8} mol of PdOEP or PtTPBP and 2.0×10^{-6} mol of DPA, BDP-G or BDP-Y were carefully solubilized in toluene. The solvent was evaporated from the homogeneous lavender organic solution by means of a gently nitrogen flow and subsequently under vacuum. The solid residue was then dissolved under magnetic stirring with 5 mL of HCl (0.85 mol L^{-1}). TEOS (100 μL) was then added to the resulting aqueous solution followed by DEDMS (20 μL) after 6 h. The mixture was kept under stirring for 48 h at 25 °C before dialysis/ultrafiltration treatments and measurements.

Characterization. Dynamic laser scattering (DLS) measurements were carried out at 25 °C on a commercial laser light scattering instrument (Malvern Autosizer 4700) at 90° scattering angle. The refractive index is 1.333 and 1.472 for water and soybean oil, respectively. The measured time correlation functions were analyzed by Automatic Program provided by Malvern. Apparent z-average hydrodynamic diameter (D_h) and polydispersity index (PDI, μ_2/Γ^2) were obtained by CONTIN mode analysis. DLS samples were prepared freshly before the measurement by diluting the emulsion 500 times with water. Transmission electron microscopy (TEM) observations were performed on a Philips CM 120 electron microscope at an accelerating voltage of 80 kV. TEM samples were prepared by diluting the emulsion to BSA concentration of 0.004 mg mL^{-1} and depositing the diluted emulsion onto a carbon-coated copper grid. The samples were dried naturally at room temperature for 72 h. ζ-Potential measurements were performed at 25 °C on a Malvern Zeta Sizer Nano ZS90 instrument. Electrophoresis mobility was measured and ζ-potential was calculated by the Dispersion Technology Software provided by Malvern. ζ-Potential sample was prepared by adjusting the emulsion to different pH values, and then diluting the emulsion to BSA concentration of 0.02 mg mL^{-1} with the same pH aqueous solution containing 5 mmol L^{-1} NaCl. Each sample was measured three times and average data were reported. The upconversion luminescence (UCL) emission spectra were recorded on Edinburgh FLS-920 instrument, but with the excitation source using an external, adjustable 532 nm (0−500 mW) or 635-nm (0−400 mW) semiconductor laser (Changchun fs-optics Co., China) with an optic fiber accessory, instead of the Xeon source in the spectrophotometer. The photos of upconversion luminescence emission were obtained digitally on a Nikon multiple CCD Camera. UV−vis absorption spectra were recorded on a Shimadzu 3000 spectrophotometer. Upconversion luminescence lifetimes was measured with phosphorescence lifetime spectrometer (FSP920-C, Edinburgh) equipped with a tunable midband OPO pulse laser as excitation source (410−2400 nm, 10 Hz, pulse width ≤5 ns, Vibrant 355II, OPOTEK). Delayed luminescence observed in the TTA upconversion of UCNC-G in water and PtTPBP as sensitizer and BDP-G as annihilator in soybean oil, both in the presence of oxygen, excited at 635 nm and monitored at 528 nm. Prompt fluorescence lifetime of UCNC-G measured in a different experiment (excited with a 397 nm diode, the decay of the emission was monitored at 528 nm) in water in the presence of oxygen. The nanosecond time-resolved transient absorption spectra were measured using laser flash photolysis instruments (LP920,

Edinburgh Instruments, U.K.) and recorded on a Tektronix TDS 3012B oscilloscope. The lifetime values (by monitoring the decay trace of the transients) were obtained with the LP900 software. Phosphorescent lifetime studies of PtTPBP were performed with an Edinburgh FLS 920 photocounting system with a Xe lamp as the excitation source. The data were analyzed by iterative convolution of the luminescence decay profile with the instrument response function using a software package provided by Edinburgh Instruments. The video showed the UCL process of BDP-G (1.0×10^{-3} mol L^{-1}) and PtTPBP (1.0×10^{-5} mol L^{-1}) under excitation of 635-nm laser at ambient environment.

Measurement of Upconversion Luminescence Quantum Efficiency. The upconversion luminescence quantum efficiency (ϕ_{UCL}) of the upconversion nanocapsules in water was determined according to eq 1.[1b] The concentration of sensitizer and annihilator relative to water is 5.0×10^{-7} and 5.0×10^{-5} mol L^{-1}, respectively, and relative to soybean oil is 1.0×10^{-5} and 1.0×10^{-3} mol L^{-1}, respectively. The equation is multiplied by a factor of 2 in order to make the maximum quantum yield to be unity.

$$\Phi_{UCL} = 2\Phi_{std}\left(\frac{A_{std}}{A}\right)\left(\frac{I_{UCL}}{I_{std}}\right)\left(\frac{\eta}{\eta_{std}}\right)^2 \tag{1}$$

Where Φ_{UCL} and Φ_{std} stand for upconversion luminescence quantum efficiency of sample UCNC and fluorescence quantum efficiency of reference dyes, respectively. A and A_{std} stand for absorbances of the UCNC and methylene blue, respectively. I_{UCL} and I_{std} stand for integrated upconversion luminescence intensity of the UCNC and fluorescence intensity of methylene blue, respectively. η and η_{std} stand for the refractive index of water (for the UCNC) and reference solvent, respectively.

Investigation of Penetration Depth. The tissue penetration abilities of UCNC-B, UCNC-G and UCNC-Y were investigated by covering experiments of beef slices on upconversion nanocapsules, with 532 nm laser (for UCNC-B) or 635 nm laser (for UCNC-G and UCNC-Y) as the excitation source, respectively.

Upconversion Luminescence Bioimaging in Vivo and ex Vivo. To perform upconversion luminescence bioimaging, the upconversion luminescence in vivo imaging system was built. One external 0−5000 mW adjustable CW 635-nm semiconductor laser was used as the excitation source, and a cooled electron-multiplying charge-coupled device (EMCCD, Andor DU897) was used as the signal collector. After subcutaneous injection of 20 μL UCNC-G, upconversion luminescence imaging in vivo was performed under different excitation power densities (11, 86, or 220 mW cm^{-2}). For lymphatic imaging, 20 μL UCNC-G and UCNC-Y was injected intradermally into the foreclaw and hindclaw, respectively. At 30 min postinjection, upconversion luminescence lymphatic imaging in vivo was performed under excitation at 635 nm (the power density of 12.5 mW cm^{-2}) when UCL emission at 530 ± 25 nm was collected with band-pass filter. For ex vivo imaging, lymph node were harvested from mice injected with the UCNC-G and UCNC-Y, respectively, for 30 min. Signal to noise ratio (SNR) = [(mean luminescence intensity of region 1 or 2) − (mean luminescence intensity of region 4)]/[(mean luminescence intensity of region 3) − (mean luminescence intensity of region 4)].

Histology Study. Tissue samples were harvested from mice injected with the UCNC-G 30 min postinjection. The lymph node was fixed in glutaraldehyde, embedded in paraffin, sectioned, and stained with hematoxylin and eosin. The histological sections were observed under an optical microscope.

■ ASSOCIATED CONTENT

Ⓢ Supporting Information

PL spectra of UCNC-Y and PtTPBP/BDP-Y enclosed in SiO$_2$, excitation with 365 nm; absorption and UCL spectra of PdOEP/DPA in soybean oil; the phosphorescent lifetime of PtTPBP; lifetime of triplet state energy level of PtTPBP in soybean oil; size distribution of UCNC-B and UCNC-Y;

5036

dx.doi.org/10.1021/ja3104268 | J. Am. Chem. Soc. 2013, 135, 5029−5037

absorption and PL spectrum of UCNC-B, UCNC-Y, and UCNC-Y in water; continuous kinetic scan of UCNC-G; the relationship between UCL and the concentration of BDP-G in PtTPBP/BDP-G system This material is available free of charge via the Internet at http://pubs.acs.org.

■ AUTHOR INFORMATION

Corresponding Author
fyli@fudan.edu.cn

Author Contributions
[#]Q.L. and B.Y.: These authors contributed to this work equally.

Notes
The authors declare no competing financial interest.

■ REFERENCES

(1) (a) Zhou, J.; Liu, Z.; Li, F. Y. *Chem. Soc. Rev.* **2012**, *41*, 1323–1349. (b) Singh-Rachford, T. N.; Castellano, F. N. *Coord. Chem. Rev.* **2010**, *254*, 2560–2573. (c) Wang, F.; Liu, X. G. *Chem. Soc. Rev.* **2009**, *38*, 976–989. (d) Schäfer, H.; Haase, M. *Angew. Chem., Int. Ed.* **2011**, *50*, 5808–5829. (e) He, G. S.; Tan, L. S.; Zheng, Q.; Prasad, P. N. *Chem. Rev.* **2008**, *108* (4), 1245–1330. (f) Wang, F.; Han, Y.; Lim, C. S.; Lu, Y. H.; Wang, J.; Xu, J.; Chen, H. Y.; Zhang, C.; Hong, M. H.; Liu, X. G. *Nature* **2010**, *463*, 1061–1065. (g) Feng, W.; Sun, L. D.; Zhang, Y. W.; Yan, C. H. *Coord. Chem. Rev.* **2010**, *254*, 1038–1053. (h) Wang, G. F.; Peng, Q.; Li, Y. D. *Acc. Chem. Res.* **2011**, *44*, 322–332.

(2) (a) Liu, Y. S.; Tu, D. T.; Zhu, H. M.; Li, R. F.; Luo, W. Q.; Chen, X. Y. *Adv. Mater.* **2010**, *22*, 3266–3271. (b) Chatteriee, D. K.; Rufalhah, A. J.; Zhang, Y. *Biomaterials* **2008**, *29*, 937–943. (c) Nyk, M.; Kumar, R.; Ohulchanskyy, T. Y.; Bergey, E. J.; Prasad, P. N. *Nano Lett.* **2008**, *8*, 3834–3838. (d) Liu, Q.; Sun, Y.; Yang, T. S.; Feng, W.; Li, C. G.; Li, F. Y. *J. Am. Chem. Soc.* **2011**, *133*, 17122–17125. (e) Yao, L. M.; Zhou, J.; Liu, J. L.; Feng, W.; Li, F. Y. *Adv. Funct. Mater.* **2012**, *22*, 2667–2672. (f) Feng, W.; Sun, L. D.; Zhang, Y. W.; Yan, C. H. *Small* **2009**, *5*, 2057–2060. (g) Cheng, L.; Yang, K.; Li, Y. G.; Chen, J. H.; Wang, C.; Shao, M. W.; Lee, S. T.; Liu, Z. *Angew. Chem., Int. Ed.* **2011**, *50*, 7385–7390.

(3) (a) Keivanidis, P. E.; Baluschev, S.; Miteva, T.; Nelles, G.; Scherf, U.; Yasuda, A.; Wegner, G. *Adv. Mater.* **2003**, *15*, 2095–2098. (b) Baluschev, S.; Miteva, T.; Yakutkin, V.; Nelles, G.; Yasuda, A.; Wegner, G. *Phys. Rev. Lett.* **2006**, *97*, 143903. (c) Baluschev, S.; Yakutkin, V.; Miteva, T.; Avlasevich, Y.; Chernov, S.; Aleshchenkov, S.; Nelles, G.; Cheprakov, A.; Yasuda, A.; Müllen, K.; Wegner, G. *Angew. Chem., Int. Ed.* **2007**, *46*, 7693–7696. (d) Islangulov, R. R.; Castellano, F. N. *Angew. Chem., Int. Ed.* **2006**, *45*, 5957–5959. (e) Islangulov, R. R.; Lott, J.; Weder, C.; Castellano, F. N. *J. Am. Chem. Soc.* **2007**, *129*, 12652–12653. (f) Zhao, W.; Castellano, F. N. *J. Phys. Chem. A* **2006**, *110*, 11440–11445. (g) Wu, W. H.; Wu, W. T.; Ji, S. M.; Guo, H. M.; Song, P.; Han, K. L.; Chi, L. N.; Shao, J. Y.; Zhao, J. Z. *J. Mater. Chem.* **2010**, *20*, 9775–9786. (h) Zhao, J. Z.; Ji, S. M.; Guo, H. M. *RSC Adv.* **2011**, *1*, 937–950. (i) Haefele, A.; Blumhoff, J.; Khnayzer, R. S.; Castellano, F. N. *J. Phys. Chem. Lett.* **2012**, *3*, 299–303.

(4) (a) Kim, J. H.; Deng, F.; Castellano, F. N.; Kim, J. H. *Chem. Mater.* **2012**, *24*, 2250–2252. (b) Singh-Rachford, T. N.; Nayak, A.; Muro-Small, M. L.; Goeb, S.; Therien, M. J.; Castellano, F. N. *J. Am. Chem. Soc.* **2010**, *132*, 14203–14211. (c) Ji, S. M.; Guo, H. M.; Wu, W. T.; Wu, W. H.; Zhao, J. Z. *Angew. Chem., Int. Ed.* **2011**, *50*, 8283–8286. (d) Wu, W. H.; Guo, H. M.; Wu, W. T.; Ji, S. M.; Zhao, J. Z. *J.* *Org. Chem.* **2011**, *76*, 7056–7064. (e) Baluschev, S.; Yakutkin, V.; Miteva, T.; Wegner, G.; Roberts, T.; Nelles, G.; Yasuda, A.; Chernov, S.; Aleshchenkov, S.; Cheprakov, A. *New J. Phys.* **2008**, *10*, 013007. (f) Guo, H.; Li, Q.; Ma, L.; Zhao, J. Z. *J. Mater. Chem.* **2012**, *22*, 15757–15768. (g) Kim, J. H.; Kim, J. H. *J. Am. Chem. Soc.* **2012**, *134*, 17478–17481. (h) Singh-Rachford, T. N.; Castellano, F. N. *J. Phys. Chem. Lett.* **2009**, *1*, 195–200. (i) Kang, J.-H.; Reichmanis, E. *Angew. Chem., Int. Ed.* **2012**, *51*, 11841–11844.

(5) Liu, Q.; Yang, T. S.; Feng, W.; Li, F. Y. *J. Am. Chem. Soc.* **2012**, *134*, 5390–5397.

(6) (a) Monguzzi, A.; Frigoli, M.; Larpent, C.; Tubino, R.; Meinardi, F. *Adv. Funct. Mater.* **2012**, *22*, 139–143. (b) Tanaka, K.; Inafuku, K.; Chujo, Y. *Chem. Commun.* **2010**, *46*, 4378–4380. (c) Turshatov, A.; Busko, D.; Baluschev, S.; Miteva, T.; Landfester, K. *New J. Phys.* **2011**, *13*, 083035. (d) Baluschev, S.; Wohnhaas, C.; Turshatov, A.; Mailander, V.; Lorenz, S.; Miteva, T.; Landfester, K. *Macromol. Biosci.* **2011**, *11*, 772–778.

(7) (a) Loudet, A.; Burgess, K. *Chem. Rev.* **2007**, *107*, 4891–4932. (b) Ulrich, G.; Ziessel, R.; Harriman, A. *Angew. Chem., Int. Ed.* **2008**, *47*, 1184–1201. (c) Kamkaew, A.; Lim, S. H.; Lee, H. B.; Kiew, L. V.; Chung, L. Y.; Burgess, K. *Chem. Soc. Rev.* **2013**, *42*, 77–88. (d) Ooyama, Y.; Okamoto, T.; Yamaguchi, T.; Suzuki, T.; Hayashi, A.; Yoshida, K. *Chem.—Eur. J.* **2006**, *12*, 7827–7838. (e) Ooyama, Y.; Kagawa, Y.; Harima, Y. *Eur. J. Org. Chem.* **2007**, 3613–3621. (f) Lu, H.; Wang, Q.; Gai, L.; Li, Z.; Deng, Y.; Xiao, X.; Lai, G.; Shen, Z. *Chem.—Eur. J.* **2012**, *18*, 7852–7861.

(8) Singh-Rachford, T. N.; Lott, J.; Weder, C.; Castellano, F. N. *J. Am. Chem. Soc.* **2009**, *131*, 12007–12014.

(9) Ziessel, R.; Singh-Rachford, T. N.; Haefele, A.; Castellano, F. N. *J. Am. Chem. Soc.* **2008**, *130*, 16164–16165.

(10) Han, Y. S.; Shchukin, D.; Yang, J.; Simon, C. R.; Fuchs, H.; Mohwald, H. *ACS Nano* **2010**, *4*, 2838–2844.

(11) Du, Y. Z.; Weng, Q.; Yuan, H.; Hu, F. Q. *ACS Nano* **2010**, *4*, 6894–6902.

(12) Yin, B. R.; Xu, K. K.; Huang, L. W.; Yao, P. *J. Colloid Interface Sci.* **2012**, *380*, 51–59.

(13) (a) Dickinson, E. *Soft Matter* **2008**, *4*, 932–942. (b) Dickinson, E.; Semenova, M. G. *Colloids Surf.* **1992**, *64*, 299–310.

(14) Goodman, C. M.; McCusker, C. D.; Yilmaz, T.; Rotello, V. M. *Bioconjugate Chem.* **2004**, *15*, 897–900.

(15) Singh-Rachford, T. N.; Castellano, F. N. *J. Phys. Chem. A* **2008**, *112*, 3550–3555.

(16) Olmsted, J. *J. Phys. Chem.* **1979**, *83*, 2581–2584.

(17) (a) Qi, J. N.; Yao, P.; He, F.; Yu, C. L.; Huang, C. *Int. J. Pharm.* **2010**, *393*, 176–184. (b) Li, J.; Yao, P. *Langmuir* **2009**, *25*, 6385–6391.